MIT Libraries | DSpace@MIT

MIT Open Access Articles

Buoyant flows in street canyons: Comparison of RANS and LES at reduced and full scales

Massachusetts Institute of Technology

Buoyant Flows in Street Canyons: Comparison of RANS and LES at Reduced and Full Scales

Lup Wai Chew[a,*], Leon R. Glicksman[a,b], Leslie K. Norford[b]

[a] Department of Mechanical Engineering, Massachusetts Institute of Technology, 77 Massachusetts Avenue, Cambridge, MA 02139, USA.

[b] Department of Architecture, Massachusetts Institute of Technology, 77 Massachusetts Avenue, Cambridge, MA 02139, USA.

* Corresponding author. 77 Massachusetts Avenue, 5-418, Cambridge, MA 02139, USA.
   E-mail addresses: lupwai@mit.edu (L. W. Chew), glicks@mit.edu (L. R. Glicksman), lnorford@mit.edu (L. K. Norford)

ABSTRACT

Reduced-scale experiments and full-scale field measurements show contradictory buoyancy effects from heated windward walls. Reduced-scale experiments exhibit significant thermal effects, but full-scale field measurements show a negligible thermal effect on the overall flow fields. This paper investigates this discrepancy by using at both scales Computational Fluid Dynamics simulations with Reynolds-Averaged Navier-Stokes (RANS) and Large Eddy Simulation (LES). Compared to experimental and field measurements, RANS models perform well at reduced scale but over-predict the thermal effects of heated windward walls at full scale. On the other hand, LES results agree well with measurements at both scales. Therefore, LES should be used for full-scale simulations of street canyon flows with heated windward walls. To date, there has been no explanation for the discrepancy of opposing thermal effects between reduced-scale experiments and full-scale field measurements although Richardson number similarity is satisfied. We provide an explanation by showing that in reduced-scale experiments with heated windward walls, the assumption of Reynolds number independence is invalid. In canyon flows with thermally induced buoyancy, unless the flow is proven independent of both Reynolds number and Grashof number, we should not generalize results from reduced-scale experiments to full-scale street canyons.

Keywords: Urban street canyon, Large Eddy Simulation, Reynolds number independence, Dimensionless group similarity, Full-scale simulation, Buoyant flow

Highlights

- Reynolds number independence assumption is invalid in flows with opposing buoyancy
- LES results match experiments at both reduced scale and full scale
- RANS results match experiments at reduced scale but not at full scale

Symbols

g [m/s^2]   gravitational acceleration

Gr [-]   Grashof number

H [m]   height of street canyon

k [m^2/s^2]   turbulence kinetic energy

L [m]   (span-wise) length of street canyon

Pr [-]   Prandtl number

r [-]   ratio of the size of the buoyancy-driven vortex to the canyon size

Re [-]   Reynolds number

Ri [-]   Richardson number

T_{ref} [K]	reference temperature
U_b [m/s]	buoyant velocity
U_{mag} [m/s]	velocity magnitude
U_{ref} [m/s]	reference velocity
$\overline{w_+}$ [m/s]	mean positive vertical velocity at the roof level
W [m]	width of street canyon
x [m]	horizontal distance from the mid-canyon axis
y^+ [-]	dimensionless wall distance
z [m]	vertical distance from the ground
ΔT [K]	temperature difference between a heated surface and the ambient air
ε [m^2/s^3]	turbulence dissipation rate
v [m^2/s]	kinematic viscosity
τ [s]	advection time scale

1. Introduction

The buoyancy effects from heated surfaces (e.g., exterior building walls) on urban wind fields remain a subject of debate. On one hand, some studies have claimed that buoyant flows induced by heated surfaces could significantly alter the overall flow fields in street canyons [1–6]. For example, heated surfaces are found to induce secondary vortices in street canyons [1–3] or eliminate a vortex that exists under isothermal conditions [6]. On the other hand, other studies have found no significant effect from heated surfaces on the overall flow fields [7–10]. For example, field measurements reveal that it is "surprising that there is no obvious effect" from the heated wall on the overall airflow pattern [9], and the thermal boundary layer thickness is on the order of 10^{-2} m, a few orders of magnitude smaller than the widths of full-scale street canyons (10^1 to 10^2 m) [10]. The discrepancy of thermal effects arises from the difference in scale: thermal effects are significant in reduced-scale experiments such as wind tunnel experiments, but thermal effects are negligible in full-scale field measurements. To satisfy similarities between these two scales, two dimensionless parameters, namely the Reynolds number and the Richardson number, should be matched.

The Reynolds number, Re, is defined as HU_{ref}/v, where H is the canyon height, U_{ref} is a reference velocity taken $2H$ or higher [11–13], and v is the kinematic viscosity. In full-scale built environments, buildings have H on the order of 10^1 to 10^2 m. With a reference wind speed of 2 m/s, the corresponding Re is on the order of 10^6 to 10^7. On the other hand, in reduced-scale experiments, scaled-down models representing buildings in a wind tunnel have H on the order of 10^{-2} to 10^{-1} m, which is two to four orders of magnitude smaller than H of full-scale buildings. In order to satisfy Re similarity, the wind speeds required in wind tunnel experiments are two to four orders of magnitude higher (200 m/s to 20,000 m/s), no longer satisfying the incompressible regime. Hence, it is not feasible to satisfy Re similarity in reduced-scale experiments. The mismatch of Re between reduced-scale experiments and full-scale field measurements is often justified by the Re independence criterion. This criterion states that beyond a critical Re, the overall flow pattern is independent of Re. Many studies of street canyon flows have adopted a critical Re of 1×10^4 [12–15]. This means that reduced-scale experiments are expected to reproduce the flow fields at full scale, as long as the Re exceeds 1×10^4.

The Richardson number, Ri, is defined as $(gH\Delta T/T_{ref})/(U_{ref})^2$, where g is the gravitational acceleration, H the canyon height, ΔT a temperature difference, T_{ref} and U_{ref} the reference temperature and velocity. The inverse of Ri, which is sometimes called the Froude number, is also commonly used in the literature [3,9,16]. In the definition of Ri, ΔT could be the temperature difference between: the leeward and windward walls [4,17]; the air at the roof level and the air at the street level [18,19]; or a surface and the ambient air [20,21]. Since we are interested in the effect of a heated wall on the ambient air, we define Ri with ΔT as the temperature difference between the ambient air and the heated wall. This definition of Ri compares the mechanical driving force to the buoyant driving force. For "skimming flow" across two-dimensional (2D) canyons [22], the mechanical force from the freestream wind drives a quasi-steady rotating vortex, as shown in Fig. 1(a). This mechanical force is proportional to Re. On the other hand, when an exterior building wall is heated by solar radiation, the buoyancy force drives an upward flow near the heated wall, as shown in Fig. 1(b). This buoyancy force is proportional to the Grashof number, Gr, which is defined as $(gH^3\Delta T)/(v^2 T_{ref})$. Since the buoyant velocity, U_b, scales with $(gH\Delta T/T_{ref})^{1/2}$, $Gr = (U_b H/v)^2$, which is the square of an equivalent Reynolds number in natural convection flows [23]. If we combine the flow fields in Fig. 1(a) and Fig. 1(b), where the windward wall (the wall facing the incoming wind) is heated, the mechanical force from the freestream wind drives a downward flow near the windward wall, but the buoyancy force drives an upward flow. These two forces thus oppose each other. Ri is the ratio of the thermal force to the mechanical force, or simply $Ri = Gr/Re^2$. When Ri is on the order of one, we expect both forces to be important. Although we cannot match the Re between reduced-scale and full-scale studies, Ri can often be matched. For example, in a full-scale street canyon with $H = 10$ m, $\Delta T = 10$ K, $T_{ref} = 300$ K, and $U_{ref} = 5$ m/s, the corresponding $Ri = 0.83$. To match this Ri with a reduced-scale model of $H = 0.2$ m while maintaining T_{ref} at 300 K, we can set $\Delta T = 80$ K and $U_{ref} = 2$ m/s. Both are achievable in wind tunnels.
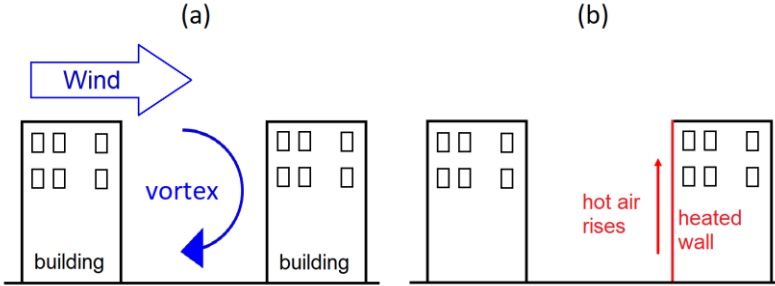

Fig. 1. (a) Freestream wind drives a quasi-steady rotating vortex, where the flow near the windward wall is directed downward. (b) When the windward wall is heated, buoyancy drives an upward flow near the windward wall.

This paper focuses on the flow fields in street canyons with opposing buoyancy effects, where the windward walls are heated. There are three common methods to study flows across street canyons, namely reduced-scale experiments, full-scale field measurements, and Computational Fluid Dynamics (CFD) simulations. The first two methods have led us to very different conclusions: the buoyancy effect is important at reduced scale [1–6] but not at full scale [7–10]. As discussed, only the Ri but not the Re (and Gr) can be matched between reduced-scale experiments and full-scale field measurements. The third method, CFD simulations, has the strength to model any Ri and Re. There are two major approaches to model street canyon flows with CFD, namely Reynolds-Averaged Navier-Stokes (RANS) and Large Eddy Simulation (LES). RANS is much more commonly used in urban wind field simulations due to its low computational cost, but LES produces results that are more accurate [24–29]. Most studies have used RANS, but it has a major drawback: while it correctly predicts significant thermal effects in reduced-scale canyons, it also predicts significant thermal effects in full-scale canyons that are inconsistent with field measurements. For example, no buoyancy-induced secondary vortices were observed in field measurements [8,9], but RANS simulations at full scale have predicted large buoyancy-induced secondary vortices [8,30]. Although comparisons between RANS and LES are available in the literature

[27,31,32], we have not found such a comparison for street canyon flows with opposing buoyancy effects. There is also no explanation for the discrepancy of opposing thermal effects between reduced-scale experiments and full-scale field measurements although Ri similarity is satisfied. In this paper, we investigate the accuracy of LES and RANS (both steady RANS and unsteady RANS or URANS) to simulate these flows by comparing their results to experimental data. We also attempt to provide an explanation for the discrepancy of opposing thermal effects at different scales. Section 2 outlines wind tunnel experiments and field measurements used to compare with CFD simulations. Section 3 describes the CFD models. Section 4 compares the simulation results to experiments, followed by discussion of the results in Section 5. Section 6 summarizes the conclusions.

2. Wind Tunnel Experiments and Field Measurements

This section provides a brief description of the wind tunnel experiments and field measurements used for CFD model evaluations. For the reduced-scale case, the wind tunnel experiments in Allegrini et al. [3] were used. The street canyon model had height $H = 0.2$ m, width $W = 0.2$ m and length $L = 1.8$ m, with a unit aspect ratio, H/W. The case with the most profound thermal effect had a reference velocity (U_{ref}) of 0.68 m/s and a reference temperature (T_{ref}) of 296 K. All surfaces were maintained at 296 K except the windward wall, which was heated to 403 K. The Re was 9,000 and the Ri was 1.54 (note that Allegrini et al. [3] adopted the inverse of Ri, which is the Froude number, in their study). An isothermal (i.e., $Ri = 0$) flow with the same Re was run as a control case. Particle image velocimetry was used to measure the flow field with a sampling frequency of 4 Hz and sampling time of 75 s.

For the full-scale cases, the field measurements in Offerle et al. [9] and Louka et al. [8] were used. The street canyon in Offerle et al. [9] is located in Gothenburg, Sweden. It has $H = 15.0$ m, $W = 7.1$ m, and $L = 50$ m, with $H/W = 2.1$. This case has $U_{ref} = 2.71$ m/s with a corresponding $Re = 2.7 \times 10^6$, and $T_{ref} = 293$ K. Taking an average windward wall temperature of 306.5 K, the corresponding Ri is 0.59. Sonic anemometers were used to measure the wind speeds and directions at eleven locations, while thermocouples were used to measure surface temperatures. A corresponding study of isothermal flow across the same street canyon is presented in Eliasson et al. [33]. The field measurement in Louka et al. [8] was conducted in a street canyon in Nantes, France. It is slightly asymmetrical, flanked by a 19.4 m tall west building and a 22.8 m tall east building. The mean $H = 21.1$ m, $W = 14.85$ m, $L = 800$ m (note that L is not given in Louka et al. [8] but they referred the readers to Vachon et al. [34] for the canyon dimension), and $H/W = 1.4$. This case has $U_{ref} = 1.44$ m/s with a corresponding $Re = 2.1 \times 10^6$, and $T_{ref} = 289$ K. Taking an average windward wall temperature of 301.6 K, the corresponding Ri is 4.42. Sonic anemometers and propellers anemometers were used to measure the wind speeds and directions at six locations, while thermocouples were used to measure surface temperatures. There is no corresponding measurement of isothermal flow for this case.

The parameters of the three cases are summarized in Table 1. Case 1 has an Ri on the order of 1. Case 2 has an Ri about three times lower than Case 1, while Case 3 has an Ri about three times higher than Case 1. The difference in Re is much larger: Case 2 and Case 3 have Re two orders of magnitude larger than Case 1.

Table 1. The parameters of the three cases: canyon height, H; height-to-width aspect ratio, H/W; reference (freestream) velocity, U_{ref}; reference (freestream) temperature, T_{ref}; Reynolds number, Re; and Richardson number, Ri.

Case	Reference	H (m)	H/W	U_{ref} (m/s)	T_{ref} (K)	Re	Ri
1	Allegrini et al. [3]	0.2	1.0	0.68	296	9,000	1.54
2	Offerle et al. [9]	15.0	2.1	2.71	293	2.7×10^6	0.59
3	Louka et al. [8]	21.1	1.4	1.44	289	2.1×10^6	4.42

3. Computational Fluid Dynamics Models

For each case in Table 1, we conducted three sets of simulations with RANS, URANS, and LES. All simulations were conducted with the finite-volume solver ANSYS Fluent (version R17.2). The standard k-ε turbulence closure scheme was used for the RANS and URANS simulations. The standard k-ε scheme does not resolve the turbulence but parametrizes the turbulence generation and turbulence dissipation to model the turbulence viscosity [35]. Following the best practice guidelines for LES in Menter [36], the SIMPLEC (Semi-Implicit Method for Pressure-Linked Equations-Consistent) algorithm was used for pressure-velocity coupling. For discretization, the Least Squares Cell Based method was used for gradients, the PREssure STaggering Option (PRESTO!) scheme was used for pressure, and the Bounded Central Differencing scheme was used for convection terms. The Bounded Second Order Implicit scheme was used for transient formulation. The Boussinesq approximation was used to model natural convection, where the density is a constant except for the body force term. The same schemes were used for the RANS and URANS simulations, except for convection terms, where the second order upwind scheme was used.

The initial temperature was set according to the freestream air temperature (T_{ref}) in each case (296 K, 293 K, and 289 K), while all other variables had zero initial conditions. Air properties at their respective T_{ref} were used in each case. The tolerance settings were as follows: 10^{-3} for continuity; 10^{-4} for velocities, turbulence kinetic energy (k), and turbulence dissipation rate (ε); and 10^{-6} for energy. These tolerance settings were verified to be sufficient by a sensitivity test with one order of magnitude smaller settings (10^{-4} for continuity; 10^{-5} for velocities, k, and ε; and 10^{-7} for energy).

Table 2 lists the boundary conditions at all boundary surfaces. A constant temperature was prescribed at the inflow surface. For Case 1, the profiles of momentum were given in Allegrini et al. [3], so we matched the inflow profiles in our CFD model to their experimental profiles. For Case 2, the freestream momentum profiles were not measured in Offerle et al. [9], but the wind speed 2 m above the roof level was measured. To obtain the inflow profiles for the CFD model, a 2D RANS simulation of the same canyon was conducted with a periodic inflow and outflow boundary condition, i.e., there is an infinite number of identical canyons in the stream-wise direction. This generates a realistic inflow boundary condition, as there are many buildings upstream of the target canyon in the field measurement site. The velocity was adjusted such that the stream-wise velocity matched the measured stream-wise wind speed 2 m above the roof level. For Case 3, the wind speed 5.3 m above the mean roof level was reported. Similar to Case 2, we obtained the inflow profiles for the CFD model in Case 3 with a 2D RANS simulation with periodic inflow and outflow and matched the measured stream-wise wind speed 5.3 m above the mean roof level. For the LES, the vortex method [37] was used to generate inflow turbulence. The outflow surface has the "outflow" boundary condition. The top surface is an adiabatic, moving shear-free wall (i.e., free-slip wall). All walls (roof, leeward wall, windward wall, and ground) have a no-slip momentum boundary condition. The span-wise surfaces have a periodic boundary condition, i.e., the canyons are infinitely long in the span-wise direction. The roof and ground surfaces are adiabatic. In Case 1, the leeward wall is adiabatic and the windward wall is prescribed a constant temperature of 403 K (similar to the wind tunnel experiment). In Case 2, the temperature profiles along both the leeward and windward walls were measured in the field experiment. The leeward wall temperature is nearly constant while the windward wall temperature is approximated with a linear line, as shown in Fig. 2(a). In Case 3, we matched the temperature profiles suggested by Louka et al. [8] in their field measurement, as shown in Fig. 2(b).

Table 2. Boundary Conditions (B. C.) at all boundaries.

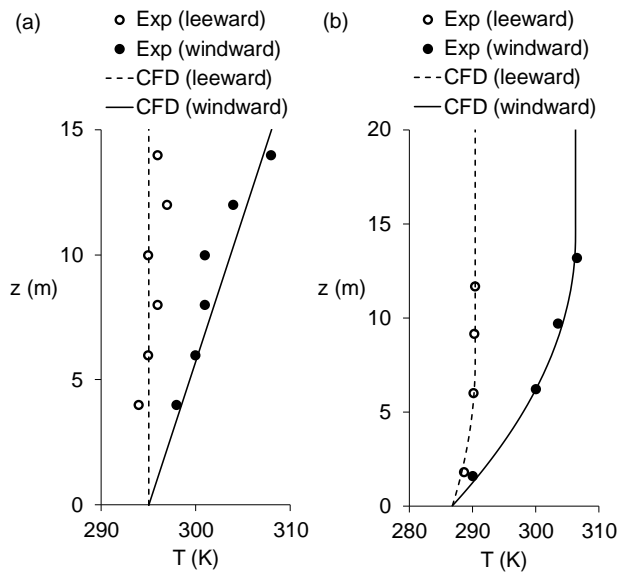| Boundary	Momentum B. C.	Energy B. C.
inflow	prescribed profiles	constant temperature
outflow	outflow	outflow
top	moving shear-free wall	adiabatic
roof	no-slip wall	adiabatic
windward wall	no-slip wall	prescribed profile
leeward wall	no-slip wall	prescribed profile or adiabatic
ground	no-slip wall	adiabatic
span-wise faces	periodic	periodic

Fig. 2. The temperature profiles at the leeward and windward walls in (a) Case 2 and (b) Case 3. The circles represent point measurements (labeled "Exp"), while the lines represent the prescribed temperature profiles (labeled "CFD") in the CFD models.

The characteristic advection timescale, τ, is defined as H/U_{ref} [38], where U_{ref} is the reference freestream velocity taken at $z/H = 2.5$, following the recommendation in the literature [11–13]. For the URANS simulation and LES, the time step size was fixed at 0.01τ [18,39]. The simulations were ramped up for 100τ before starting statistical averaging [39]. For Case 1, the averaging period was 250τ to match the averaging period in the wind tunnel experiments. For Case 2 and Case 3, the averaging periods were 100τ [39]. All three cases have Courant numbers < 1 in the canyons.

Fig. 3 shows the canyon in Case 1 modeled with ANSYS DesignModeler. The canyon has $H = W = 0.2$ m. The origin is located in the mid-canyon ($x = 0$) at the ground level ($z = 0$), where x is the distance from the mid-canyon while z is the distance from the ground. The upstream and downstream roof width is $0.5H$. The top boundary is $5H$ above the ground. The model was meshed with ANSYS Meshing and consisted of orthogonal cells with near-wall cell refinement. The smallest cells had a cell size of $0.02W$. The cell expansion ratio was smaller than 1.2. A similar approach was used to model and mesh the canyons in Case 2 and Case 3. For brevity, only the mesh of Case 1 is shown in Fig. 3. The total numbers of cells are 54,000, 84,600, and 86,500 in Cases 1-3, respectively. The three cases were tested on their respective refined meshes with 96,000, 133,600, and 163,440 cells. We use the normalized mean-square error (NMSE) in Hanna and Chang [40] to evaluate the differences between the normal and fine mesh

models. $NMSE = \overline{(u_n - u_f)^2}/(\overline{u_n} \times \overline{u_f})$, where u_n and u_f are the stream-wise velocities taken at the mid-canyon lines from the normal and fine mesh models. The over-bars represent the spatial average of the mid-canyon line profiles. Table 3 summarizes the NMSE for each case. All three cases have small NMSE (<0.01), confirming that the normal mesh resolution is sufficient to resolve the flow features.
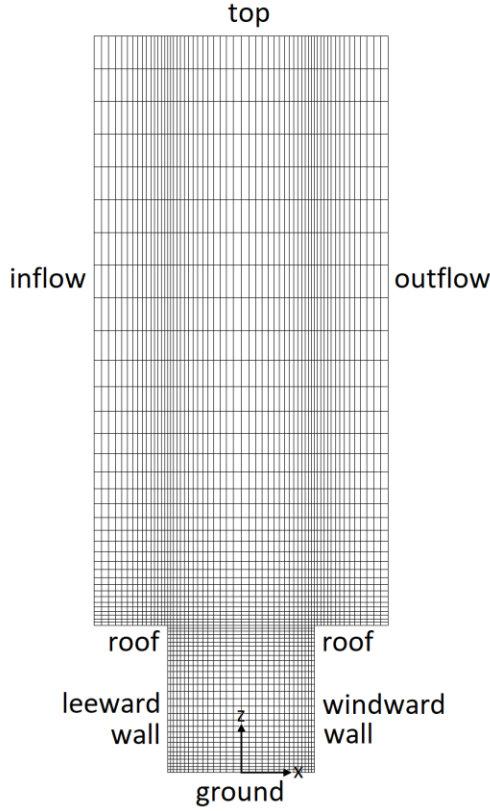

Fig. 3. The boundary names and mesh resolution of the model in Case 1 with $H = W = 0.2$ m. In the span-wise direction (into the page), $L = 0.2$ m and has 20 uniform cells.

Table 3. The normalized mean-square error (NMSE) between the normal mesh and fine mesh

Case	NMSE (RANS)	NMSE (LES)
1	0.00013	0.0011
2	0.0033	0.0081
3	0.000085	0.0076

4. Simulation Results

4.1 Case 1: Wind Tunnel Experiments of Reduced-Scale Canyon

The dimension of the canyon is the same as that in the wind tunnel experiments, except L. Since L is much larger than both H and W, we modeled the canyon as $H = 0.2$ m, $W = 0.2$ m and $L = 0.2$ m with a periodic span-wise boundary condition to simulate an infinitely long canyon in the span-wise direction. This reduced-scale case has a relatively small length scale so the average dimensionless wall distance, y^+, was small at 3.6. No wall function was used for the LES simulation. For the RANS and URANS simulations, the recommended Enhanced Wall Treatment [41] was used. The τ for this case is $H/U_{ref} = 0.2/0.68 \approx 0.3$ s. The URANS simulation and LES for this case had a fixed time step size of $0.01\tau = 0.003$

8

s. The ramp up period was 100τ (30 s). Statistical averaging started at 30 s. We matched both the sampling frequency (4 Hz) and averaging period (75 s) in the wind tunnel experiments, so the statistical averaging was performed between 30 s and 105 s.

Fig. 4 compares the simulation results from RANS, URANS, and LES to the wind tunnel experiments. Isothermal flows were also simulated to compare with the experiment with no heated walls. For the isothermal flows, Fig. 4(b)-(d) show that RANS, URANS, and LES performed equally well in predicting the flow field observed in the wind tunnel experiment in Fig. 4(a) (note the different scale bar for the measurements). All CFD models predicted a single major vortex, consistent with the wind tunnel experiment. On the other hand, for the simulations with the windward wall heated, the experimental result in Fig. 4(e) shows that the large vortex observed in the isothermal flow has disappeared. Most of the canyon is stagnant or has very low flows (light purple and dark purple), except near the roof level and windward wall, where the flows are strong (black and light green). This suggests that the thermal effect is strong enough to counter the mechanical effect from the freestream. Overall, Fig. 4(f)-(h) show that all CFD models produced satisfactory results compared to the wind tunnel experiment. All models predicted significant thermal effects, which induce secondary vortices near the windward walls. LES performed the best by predicting a larger region of stagnant air observed in the wind tunnel experiment.
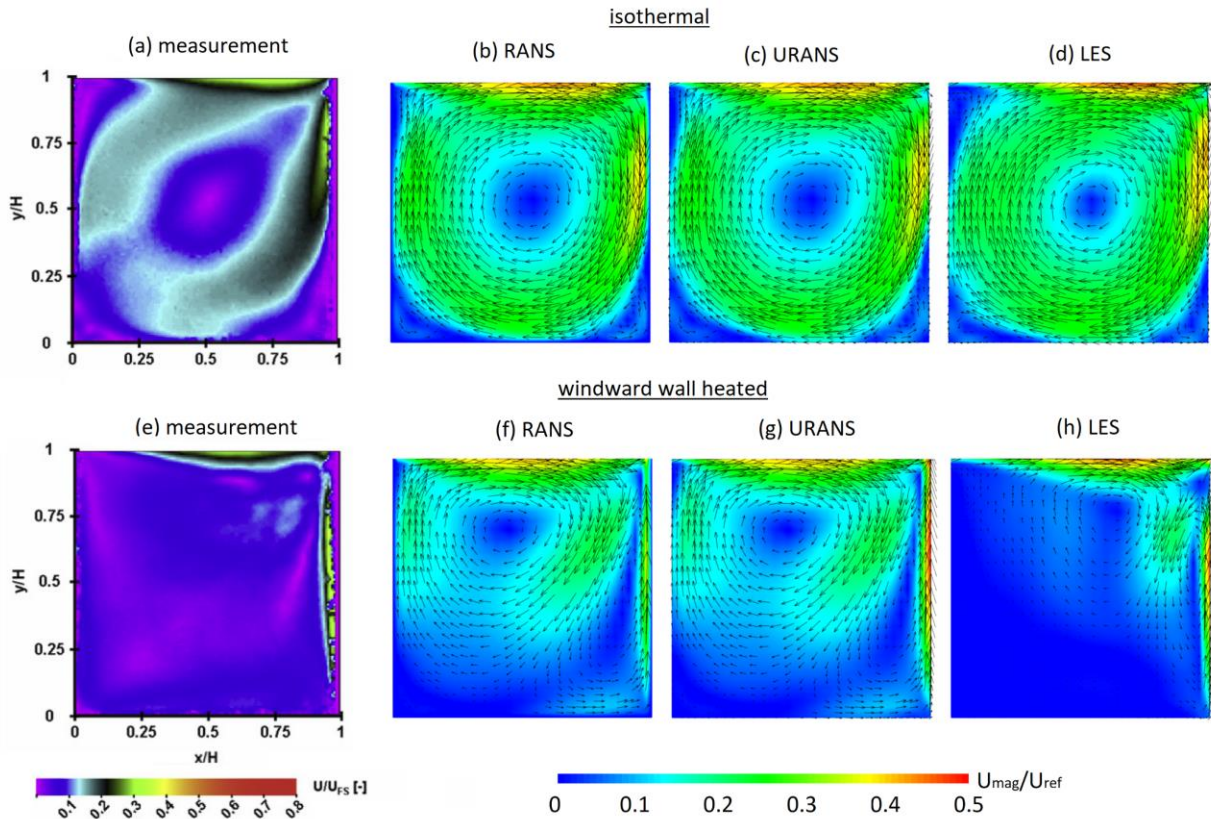

Fig. 4. Comparison of wind tunnel experiments and simulation results of Case 1 with $H = W = 0.2$ m, $Re = 9,000$, and $Ri = 1.56$. (a) Normalized velocity contours of isothermal flow from wind tunnel experiment in Allegrini et al. [3]; normalized velocity magnitude contours and vectors of isothermal flows from (b) RANS, (c) time-averaged URANS, and (d) time-averaged LES. (e) Normalized velocity contours of windward-wall-heated flow from wind tunnel experiment in Allegrini et al. [3]; normalized velocity magnitude contours and vectors of windward-wall-heated flows from (f) RANS, (g) time-averaged URANS, and (h) time-averaged LES.

4.2 Case 2: Field Measurements of a Full-Scale Canyon in Sweden

For Case 2, the dimension of the canyon in the CFD model is the same as that in the full-scale street canyon in Offerle et al. [9], except *L*, which is set to 7.1 m with a periodic span-wise boundary condition to simulate an infinitely long canyon. This full-scale case has an average y^+ of 145, which is sufficiently large to employ wall functions. The Werner and Wengle wall function [42] was used for the LES, while the standard wall function [43] was used for the RANS and URANS simulations. The τ for this case is $H/U_{ref} = 15/2.71 \approx 5.5$ s. The LES and URANS simulations for this case had a fixed time step size of $0.01\tau = 0.055$ s. Both LES and URANS simulation were ramped up 100τ to 550 s. Statistical averaging started at 550 s. The sampling frequency and sampling period were not given in the field measurements, so the averaging was performed for every time step in the CFD simulations for 100τ (i.e., 550 s to 1,100 s).

Fig. 5 compares the simulation results from RANS, URANS, and LES to the field measurements. This canyon has a high aspect ratio of 2.1, which is categorized as a "deep" canyon [44]. Although deep canyons are generally understood to induce two or more vortices [14,39,45], the multiple-vortex flow pattern is observed only in reduced-scale experiments. In full-scale canyons, only one vortex is expected at sufficiently high *Re* [46]. In fact, the full-scale field measurement assuming no thermal effect in Fig. 5(a) reveals that there is only one vortex in this deep canyon [33]. Fig. 5(b)-(d) show that under isothermal conditions, all three simulations (RANS, URANS, and LES) predicted a flow field with one vortex, consistent with the field measurement. Note that to illustrate more clearly the wind fields in the field measurements (which have only ten data points), the vector lengths in Fig. 5(a) and Fig. 5(e) have a different scale from the simulation results in Fig. 5(b)-(d) and Fig. 5(f)-(h).

When the windward wall is heated, Fig. 5(e) shows that a single vortex is observed in the field measurement [9]. Comparing the measurements between the windward-wall-heated flow in Fig. 5(e) and the isothermal flow in Fig. 5(a), the heated wall seems to have no effect on the overall flow field. However, the RANS result in Fig. 5(f) and the URANS result in Fig. 5(g) show significant thermal effects, where the clockwise rotating vortex driven by the freestream wind shrinks and occupies only the top part of each canyon. Both RANS and URANS predicted very weak flow below the vortex. Near the windward wall, an upward flow is predicted by RANS and URANS at the bottom half of the canyon, indicating relatively strong buoyancy effects. On the other hand, Fig. 5(h) shows that LES correctly predicted one major vortex, which is consistent with the single-vortex flow field observed in the field measurement in Fig. 5(e). Comparing Fig. 5(h) with Fig. 5(d), the near-ground flow in Fig. 5(h) is weaker, suggesting the heated windward wall could reduce near-ground wind speeds. Unfortunately, both field measurements [9,33] in Fig. 5(a) and Fig. 5(e) do not have data near the ground level to verify this. Overall, comparing Fig. 5(e)-(h), only the LES model predicted the flow pattern observed in the field measurement. Both RANS and URANS over-estimated the thermal effects and predicted a flow pattern significantly different from the field measurement. Some studies suggest that RANS with modified *k-ε* turbulence schemes such as the Renormalization Group (RNG) and the realizable *k-ε* could perform better [20,47–49]. We repeated the RANS simulations with both the RNG and realizable schemes. Both predicted significant thermal effects, similar to the results obtained from the standard *k-ε* scheme.
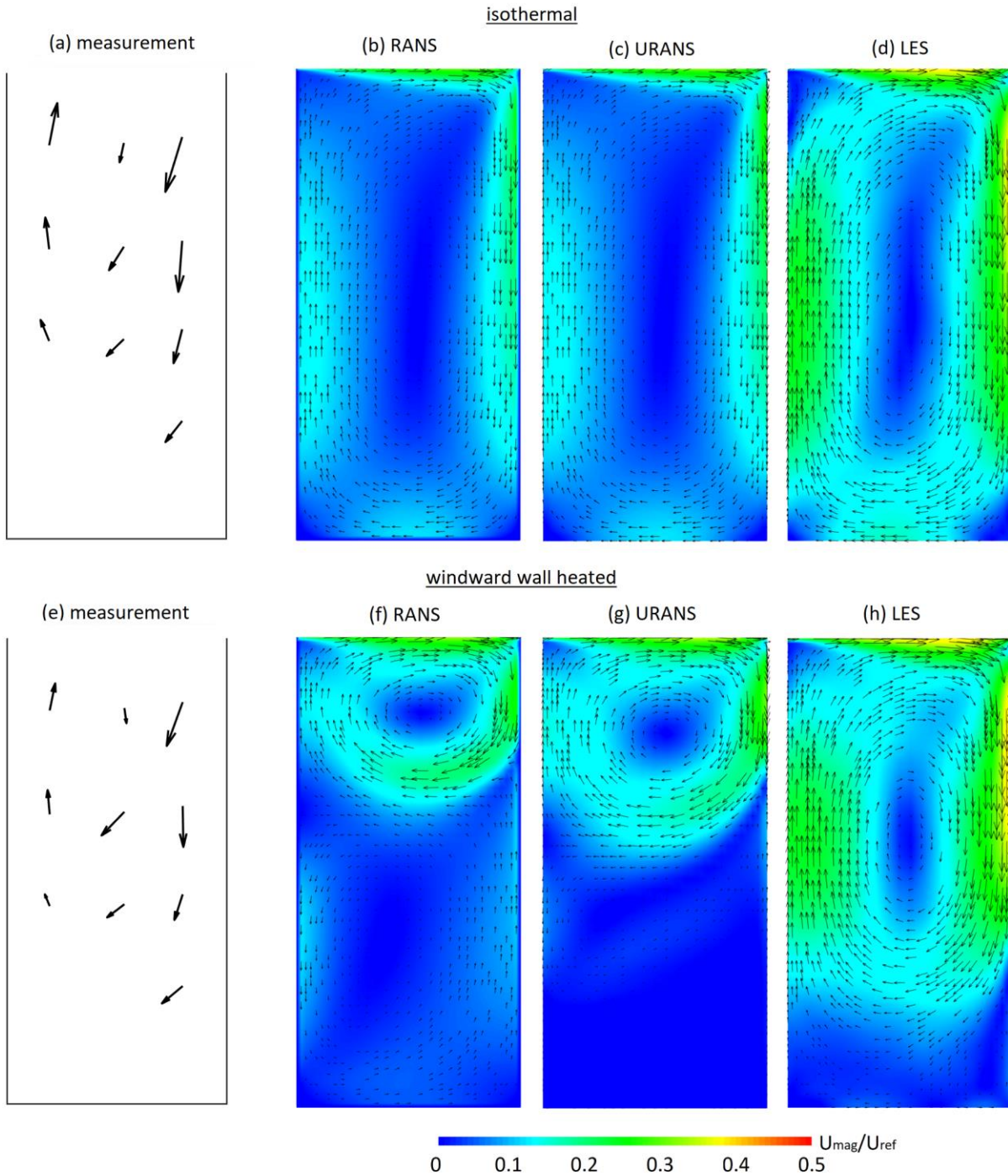
Fig. 5. Comparison of field measurements and simulation results of Case 2 with $H = 15$ m, $W = 7.1$ m, $Re = 2.7 \times 10^6$, and $Ri = 0.59$. (a) Velocity vectors in field measurement assuming isothermal condition in Eliasson et al. [33]; normalized velocity magnitude contours and vectors of isothermal flows from (b) RANS, (c) time-averaged URANS, and (d) time-averaged LES. (e) Velocity vectors in field measurement with the windward wall heated in Offerle et al. [9]; normalized velocity magnitude contours and vectors of windward-wall-heated flows from (f) RANS, (g) time-averaged URANS, and (h) time-averaged LES.

4.3 Case 3: Field Measurement of a Full-Scale Canyon in France

For Case 3, the dimension of the canyon in the CFD model is the same as that in the full-scale street canyon in Louka et al. [8], except *L*, which is set to 14.85 m with a periodic span-wise boundary condition to simulate an infinitely long canyon. The average y^+ was 258, so the Werner and Wengle wall function [42] was used for the LES, while the standard wall function was used for the RANS and URANS simulations. The τ for this case is $H/U_{ref} = 21.1/1.44 \approx 15$ s. The LES and URANS simulation for this case had a fixed time step size of $0.01\tau = 0.15$ s. Both LES and URANS simulation were ramped up 100τ to 1,500 s. Statistical averaging started at 1,500 s. The sampling frequency and sampling period were not given in the field measurement, so the averaging was performed for every time step in the CFD simulations for 100τ (i.e., 1,500 s to 3,000 s).

Fig. 6 compares the simulation results to the field measurement in Louka et al. [8]. From Fig. 6(a), the field measurement suggests a flow field with a single vortex. The RANS and URANS in Fig. 6(b) and Fig. 6(c) show weak overall flows and large regions of nearly stagnant air. The velocity vectors near the windward wall point upward, indicating a strong buoyant flow along the windward wall. This strong buoyant flow opposes the freestream wind and shrinks the clockwise rotating vortex driven by the freestream wind. The flow fields shown in Fig. 6(b) and Fig. 6(c) are significantly different from the flow field observed in the field measurement in Fig. 6(a). This indicates that RANS and URANS failed to predict the correct flow field when the windward wall was heated. On the other hand, Fig. 6(d) shows that LES predicted a flow field with a large clockwise rotating vortex, consistent with the single-vortex flow field observed in the field experiment. From the LES result, the velocity vectors near the windward wall point downward (except near the ground), indicating that the downward flow driven by the freestream wind dominates over the buoyant flow. Overall, comparing Fig. 6(a)-(d), only the LES model predicted the flow pattern observed in the field measurement. Both RANS and URANS over-estimated the thermal effects and predicted a flow pattern significantly different from the field measurement. For isothermal flow, although there is no corresponding field measurement under isothermal conditions reported in Louka et al. [8], we expect the flow field to not differ much from that in Fig. 6(d), as shown in Fig. 6(e).
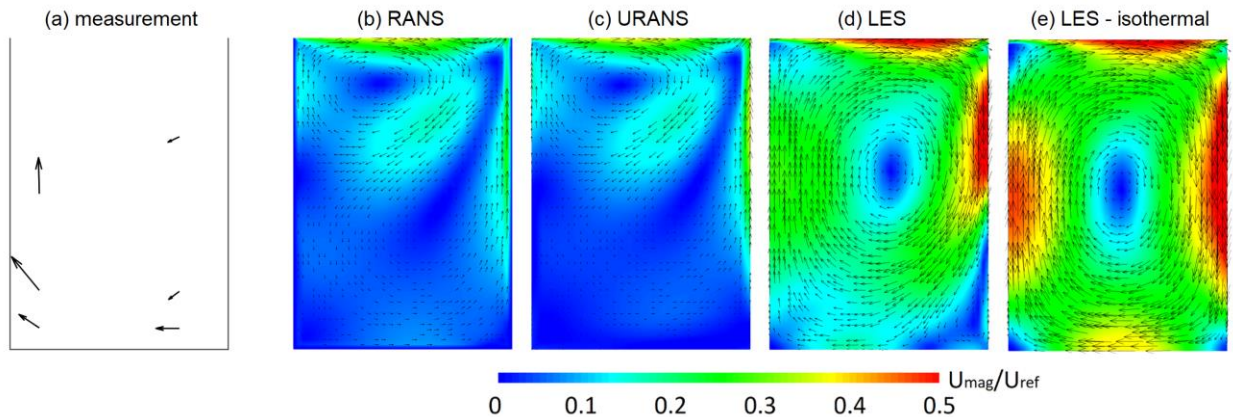

Fig. 6. Comparison of field measurement and simulation results of Case 3 with $H = 21.1$ m, $W = 14.85$ m, $Re = 2.1 \times 10^6$, and $Ri = 4.42$. (a) Velocity vectors in field measurement with the windward wall heated in Louka et al. [8]; normalized velocity magnitude contours and vectors of windward-wall-heated flows from (b) RANS, (c) time-averaged URANS, (d) time-averaged LES, and (e) time-averaged LES for isothermal flow.

5. Discussion

5.1 Performance Comparison among RANS, URANS, and LES

The wind tunnel experiments in Allegrini et al. [3] show that the thermal effect is significant at reduced scale, as depicted in Fig. 4(e). On the other hand, the field measurements in Offerle et al. [9] and Louka et al. [8] show a negligible thermal effect on the overall flow fields at full scale, as depicted in Fig.

5(e) and Fig. 6(a). Comparing the simulation results to measurements, RANS and URANS correctly predicted the flow fields with significant thermal effects at reduced scale, but failed to predict the correct flow fields at full scale. On the other hand, LES correctly predicted the flow fields at both scales. The results suggest that when the windward wall is heated, we can use RANS or URANS to model flows only at reduced scale, but not at full scale. LES should be used to predict the overall flow fields in full-scale canyons with heated windward walls. However, due to its high computational cost, LES is not always feasible, especially in simulations of large domains with many street canyons. Under such circumstances where RANS is the only viable option, simulations of isothermal flows are preferable. Although RANS simulations of isothermal flows do not provide the temperature fields, they predict the overall flow fields correctly. In contrast, full-scale RANS simulations with heated windward walls predict the wrong flow fields. Consequently, other variables that depend on the flow fields will also be incorrect. We will illustrate this with a calculation of air exchange rate (AER).

AER quantifies the ventilation performance at the roof level [50,51]. AER can be partitioned into air exchange due to mean and fluctuating vertical velocities. Fig. 4 to Fig. 6 plot the mean velocity contours so we will calculate only the mean component of AER. The total mean AER at the roof level, $\langle\overline{AER}\rangle = \int_{-W/2}^{W/2} \overline{w_+}\, dx$, where $\overline{w_+}$ is the mean positive vertical velocity at the roof level [50,51]. The integration is performed over the canyon width W (from $x = -W/2$ to $x = W/2$, see Fig. 3 for the coordinate system). The $\langle\overline{AER}\rangle$ is then normalized by dividing it with U_{ref} and W. Table 4 summarizes the normalized $\langle\overline{AER}\rangle$ in each case and the difference between isothermal flows and flows with heated wall. For Case 1, the experimental results show very different flow fields between isothermal flow (Fig. 4(a)) and flow with heated wall (Fig. 4(e)), therefore a large difference of $\langle AER\rangle$ is expected. LES predicted a larger difference than RANS, showing its superiority over RANS. For Case 2, the field measurements show similar flow fields between the isothermal flow (Fig. 5(a)) and the flow with heated wall (Fig. 5(e)), therefore a small difference of $\langle\overline{AER}\rangle$ is expected. LES predicted only 14% difference, while RANS predicted 184% difference, again showing that LES is more accurate than RANS. For Case 3, no field measurement of isothermal flow was reported, but the trend is similar to Case 2, where LES predicted a small difference at 7%, while RANS over-predicted the difference at 177%.

Table 4. Normalized $\langle\overline{AER}\rangle$ and the percentage difference between isothermal flow and flow with heated wall.

Case	RANS			LES		
	Isothermal	Heated Wall	Difference (%)	Isothermal	Heated Wall	Difference (%)
1	0.0086	0.0127	48	0.0074	0.0152	107
2	0.0025	0.0072	184	0.0070	0.0060	14
3	0.0060	0.0166	177	0.0088	0.0082	7

Why does RANS fail to predict the overall flow field at full scale when the windward wall is heated? We propose two hypotheses: flow separation and the Boussinesq approximation of the turbulence generation by buoyancy. Flow separations can occur when the forced convection flow opposes the natural convection flow [23,52]. To visualize such complex interactions involving flow separations, Fig. 7 shows five snapshots of instantaneous velocity magnitude contours and vectors from LES of Case 3. The time interval between each frame is 9 s (6τ). At 1521 s, an upward flow is developing at the bottom right corner, while a strong jet induced by the freestream is flowing downward along the windward wall. At 1530 s, this strong downward flow collides with the developing upward buoyant flow. The opposing interaction weakens both the downward and upward flows, as shown at 1539 s. At 1548 s, the upward flow has completely lost its momentum while the downward flow occupies the bottom right corner, and another strong downward jet is observed. This strong downward jet temporarily suppresses the development of the upward buoyant flow, so no upward flow is developed at the bottom right corner at

1557 s. Throughout the whole simulated period, there are many other such cycles of opposing interactions and flow separations. A video showing these cycles is included in the supplementary material, which can be found at https://doi.org/10.1016/j.buildenv.2018.09.026. The video shows the instantaneous velocity contours and vectors from 1500 s to 2250 s (real time, not CPU time), which corresponds to 100τ to 150τ. Fig. 7 proves that the flow with opposing buoyancy effects is highly unsteady with flow separations. Clearly, the steady-state solver RANS could not reproduce such unsteady flow features. Being an unsteady solver, can URANS resolve the unsteady flow features? The answer is no, as shown in the instantaneous velocity contours and vectors in Fig. 8. Comparing Fig. 8 with Fig. 7, the time instances are similar, but the flow fields at each frame are very different. URANS simulation in Fig. 8 does not resolve the flow separations. In fact, URANS solves for the unsteady mean flow but the turbulence is modeled [25] (e.g., the k-ε model used in our simulations). This brings us to the second hypothesis, which is the modelling of turbulence generation by buoyancy using the Boussinesq approximation.
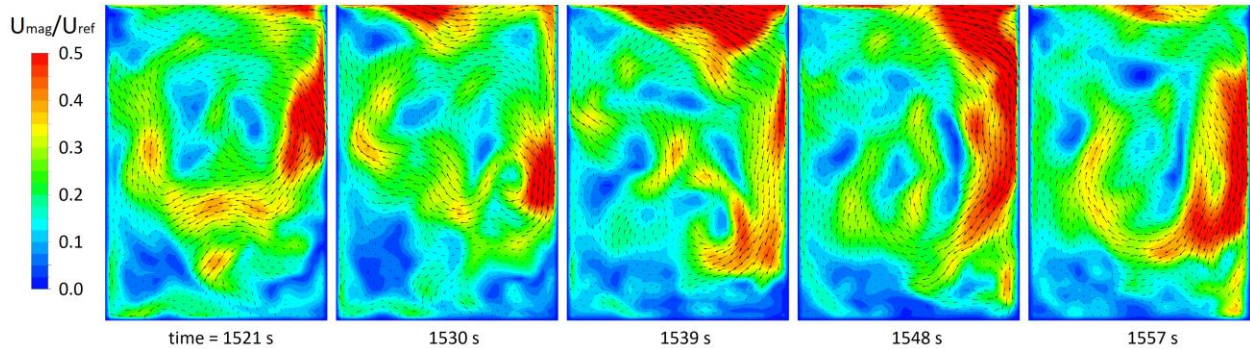

Fig. 7. Instantaneous velocity contours and vectors at different times from LES of Case 3 showing the interaction between the mechanical-driven flow and the buoyancy-driven flow. Near the heated windward wall, the opposing downward flow induced by the freestream wind and the upward flow induced by buoyancy cause flow separations.
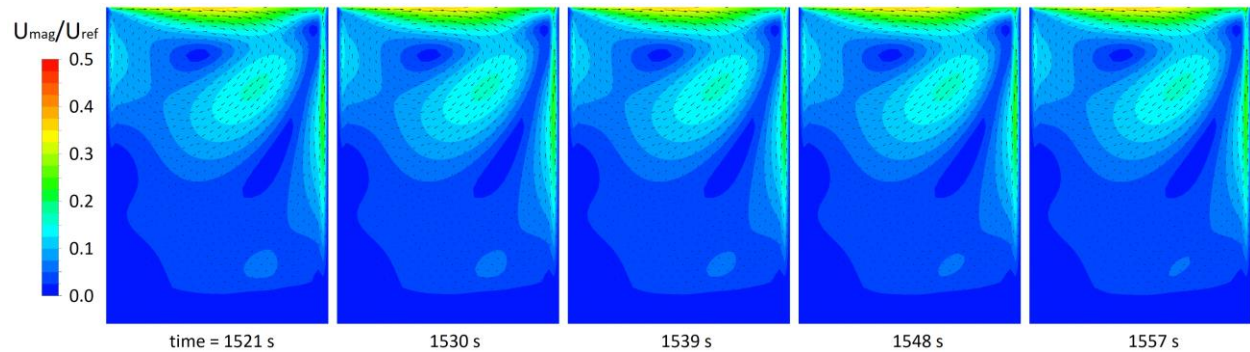

Fig. 8. Instantaneous velocity magnitude contours and vectors from URANS simulation of Case 3. The unsteady flow features including the flow separation observed in LES (see Fig. 7) were not captured by URANS.

In flows with heat transfer, turbulence can be generated by density difference and shear. As discussed in the previous paragraph, RANS models (but does not resolve) the turbulence. The general turbulence generation by density difference includes the horizontal gradients of pressure and density (temperature) [53]. In the RANS model adopted in our study, the turbulence generation by buoyancy neglects the horizontal gradients and is estimated by the Boussinesq approximation as $\mu_t g(\Delta T/H)/(T_{ref}Pr_t)$, where Pr_t is the turbulent Prandtl number (=0.85) [35]. Near the wall, the horizontal gradients are significant, invalidating the Boussinesq approximation employed by RANS. This could be the reason why RANS failed to predict the flow fields in Case 2 and Case 3. Another consequence of using the Boussinesq approximation in RANS is that the relative importance of the turbulence generation by density difference to the turbulence generation by shear is reduced to a constant (Ri). The turbulence

generation by density difference scales with $\mu_t g(\Delta T/H)/(T_{ref}Pr_t)$, while the turbulence generation by shear scales with $\mu_t(U_{ref}/H)^2$. Taking the ratio of the turbulence generation by buoyancy to the turbulence generation by shear, we get $gH\Delta T/(T_{ref}Pr_t(U_{ref})^2) = Ri/Pr_t \approx Ri$ for $Pr_t = 0.85$. In other words, Ri measures the relative importance of turbulence generation by buoyancy to turbulence generation by shear. If $Ri \ll 1$, turbulence generation by buoyancy is negligible; if $Ri \gg 1$, turbulence generation by shear is negligible. In Section 4, we have shown that the discrepancy between reduced-scale experiments and full-scale field measurements cannot be determined by Ri alone, as the thermal effects are significant at low Re but negligible at high Re. We will discuss the roles of Re in the next section.

5.2 Reynolds Number and Richardson Number Similarities

This subsection revisits the concept of Re and Ri similarities. Referring to Table 1, all cases have Ri near the order of one, but the full-scale Case 2 and Case 3 have Re two orders of magnitude higher than the reduced-scale Case 1. Case 2 and Case 3 indicate a negligible thermal effect on the overall flow fields, while Case 1 shows significant thermal effects. Since Ri similarity is satisfied, the assumption of Re independence, where a flow field does not change with increasing Re beyond a critical Re (usually taken to be on the order of 10^4), must be invalid. We believe that the critical Re of 1×10^4, originally derived for isothermal flows [54], has been incorrectly generalized to street canyon flows with heat transfer. For isothermal flows, the thermal force is absent so $Gr = 0$. Correspondingly, $Ri = Gr/Re^2 = 0$, regardless of the Re. For flows with heat transfer, Ri similarity requires the coupling of Gr and Re. When Re is increased, Gr needs to be increased, too. However, there is no Gr independence criterion, so increasing Gr (although Ri is maintained) could alter the overall flow fields. In other words, the Re independence criterion derived from isothermal flows should not be generalized to flows with heat transfer.

Let us quantify the thermal effect as a dimensionless ratio, r, of the size of the buoyancy-induced vortex to the size of canyon. From dimensional analysis, $r = f(Re, Ri, Pr, H/W)$, where f is an unknown function and Pr is the Prandtl number. Since we use the same fluid (air) at both scales and since geometrical similarity is satisfied, we can drop the dependence on Pr and H/W. Furthermore, if Re independence is valid, we can drop the dependence on Re, so r is a function of only Ri, or simply $r = f(Ri)$. However, the comparison between reduced-scale experiments and full-scale field measurements in Section 4 proves that $r = f(Ri)$ is incorrect, because when Ri is on the same order of magnitude, r is significant at Re on the order of 10^4 (Case 1) but nearly zero at Re on the order of 10^6 (Case 2 and Case 3). This means that the flows are a function of Re, at least in the studied range between 10^4 and 10^6. In other words, the Re independence assumption is not valid for Re between 10^4 and 10^6. We must retain the dependence on Re while studying the thermal effects on the flow fields, so $r = f(Re, Ri)$, or more generally, $r = f(Re, Ri, Pr, H/W)$ to account for different fluids and canyon aspect ratios used in experiments.

One may argue that the significant thermal effect at reduced scale is caused by a large absolute ΔT (107 K in Case 1), not the mismatch of Re. In other words, even if Re is matched, a large ΔT could still induce significant thermal effects at full scale. We conducted a set of LES to test this hypothesis. From the literature, the maximum recorded ΔT in full-scale canyons are 9 K [10,55], 14 K [7,56], and 18 K [8]. It is unlikely that a building surface could reach 18 K higher than the ambient air. We took a higher upper limit of ΔT of 20 K. A full-scale canyon with $H = W = 20$ m was modeled (equivalent to the canyon in Case 1 scaled up by 100 times). T_{ref} and U_{ref} were 300 K and 2 m/s. Both were realistic in a real built environment. The windward wall had a constant ΔT of 20 K. The corresponding Re and Ri were 2.6×10^6 and 3.27, close to those of Case 3. The numerical schemes outlined in Section 3 were used for the LES.

Fig. 9(b) shows the time-averaged normalized velocity contours and vectors for this test case with a canyon of $H = 20$ m. The flow field shows a single major vortex analogous to the flow field observed in an isothermal flow. Therefore, the thermal effect is insignificant in this test case. This is expected, since Case 3 with about the same Re and Ri as this test case reveals that the thermal effect is insignificant. In the next test case, H was halved to 10 m. To satisfy Re similarity, U_{ref} was doubled to 4 m/s. To satisfy Ri

similarity, ΔT was increased by eightfold to 160 K, because ΔT scales with square of U_{ref} and $1/H$. Fig. 9(a) shows the normalized flow field. Although the absolute $\Delta T = 160$ K is large (even larger than $\Delta T = 107$ K in the reduced-scale experiment in Case 1), the flow field in Fig. 9(a) is similar to that of Fig. 9(b). This confirms the applicability of dimensionless group similarities. In addition, the difference between the flow field in Fig. 9(a) to that of Fig. 4(h) further confirm that the magnitude of ΔT alone cannot determine the significance of thermal effects (in fact, the test case in Fig. 9(a) had a larger ΔT than the case in Fig. 4(h)). Lastly, we repeated the test case on a canyon with $H = 40$ m. To satisfy Re and Ri similarities, U_{ref} was reduced to 1 m/s, and ΔT was reduced to 2.5 K. Fig. 9(c) shows a similar normalized flow field as those in Fig. 9(a) and Fig. 9(b). This is expected, since both Re and Ri similarities were satisfied.
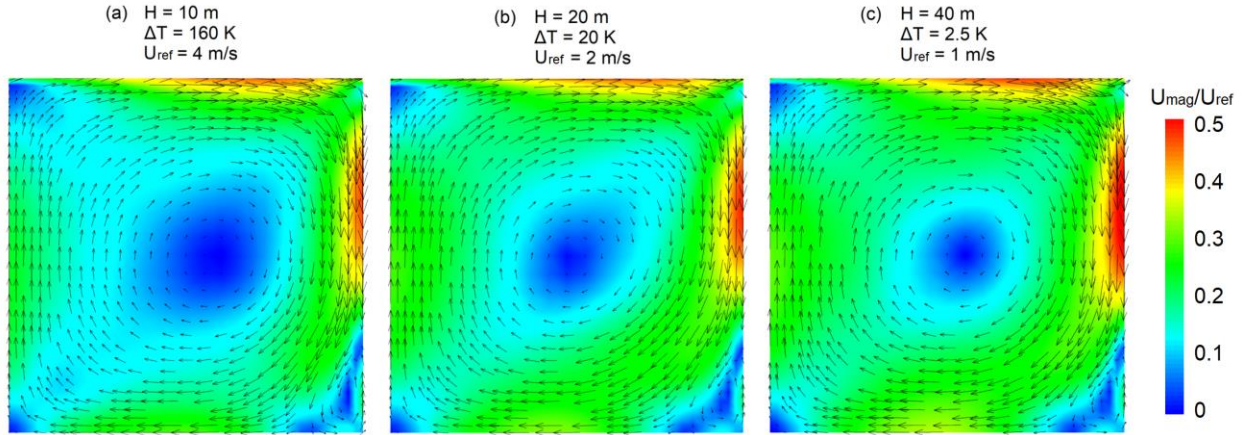

Fig. 9. Normalized velocity magnitude contours and vectors from LES of full-scale canyons with (a) $H = 10$ m, (b) $H = 20$ m, and (c) $H = 40$ m. All cases have $Re = 2.6 \times 10^6$ and $Ri = 3.27$. T_{ref} was fixed at 300 K in all three cases, while U_{ref} and ΔT were adjusted in each case to match Re and Ri.

To summarize, we have shown that the thermal effect from a heated windward wall is a function of both Re and Ri, or simply $r = f(Re, Ri)$. The Re independence criterion, where the critical Re (= 1×10^4) derived from an isothermal flow across a surface-mounted cube [54], is invalid. Although this is a simple proof that thermal effects are a function of both Re and Ri, many reduced-scale studies that include thermal effects have overlooked it and assumed Re independence in their experiments. We hope that we have provided a strong argument to reconsider the Re independence criterion in designing reduced-scale experiments of street canyon flows with heat transfer. Note that in general, $r = f(Re, Ri, Pr, H/W)$. The function f remains unknown. There may exist a dimensionless parameter π (as a combination of Re, Ri, Pr, and H/W) such that $r = f(\pi)$ will collapse to a single curve. The search for π and f, if they exist, could be an interesting future work.

5.3 Limitations of Current Study

This study focuses on perpendicular winds across 2D-like canyons (i.e., canyons with large span-wise lengths). Although the CFD simulations were conducted with 3D models, the mean span-wise velocity is nearly zero. In addition, the canyons in this study have an idealized geometry with smooth walls. In a real canyon, complex geometry and 3D features could change the local flow fields. Therefore, care must be taken to generalize the results from this study to 3D canyons.

Depending on the local time and the solar angle, the surface temperatures could differ significantly throughout a day. Under the same wind direction, either the leeward wall, the windward wall, or both walls could be heated by solar radiation. This study investigates the opposing buoyancy force (windward wall heated). In the case of assisting buoyancy force (leeward wall heated), since the mechanical and buoyant flows are in the same direction, no flow separation is expected. Although

opposing thermal effects are negligible on the overall flow fields at full scale, we should not generalize that assisting thermal effects are negligible.

As discussed in Section 5.1, turbulence modeling by the Boussinesq approximation in RANS is over-simplified, as the horizontal gradients of pressure and density (temperature) are neglected. This could be the reason RANS failed to predict the flow fields in the full-scale cases with the windward wall heated. We have not repeated the simulations by retaining the gradient terms, and this could be an interesting future work.

6. Conclusions

We conducted CFD simulations with RANS, URANS, and LES in both reduced-scale and full-scale canyons and compared the results with experimental data from wind tunnel experiments or field measurements. Under isothermal conditions (when no surface is heated), RANS, URANS, and LES predicted accurate flow fields at both reduced scale and full scale. However, with the windward wall heated (opposing buoyancy force), only LES accurately predicted the flow fields at both scales. RANS and URANS performed well at reduced scale but not at full scale.

Due to its superior performance over RANS, LES is recommended for full-scale simulations with heated windward walls. Nevertheless, LES may not be feasible to simulate such large domains as a whole city. Furthermore, Blocken [25] has highlighted that RANS will continue to remain the most common CFD approach to simulate urban wind fields. In full-scale simulations with heated windward walls, RANS overestimates the thermal effects and may fail to predict accurate wind fields. Consequently, other variables such as the air exchange rate and the temperature fields that depend on the wind fields (e.g., advection of heated air) will also be wrongly predicted. Therefore, if RANS were to be used for full-scale simulations, we recommend simulations with isothermal conditions, even in scenarios where building surfaces are heated. Obtaining a correct wind field without the temperature field is preferable to incorrect wind and temperature fields.

We revisited the Reynolds number and Richardson number similarities. The Richardson number similarity can be satisfied at reduced-scale experiments but not the Reynolds number similarity. The latter is often circumvented by the Reynolds number independence criterion, where a critical Reynolds number of 1×10^4 is "sufficiently" high to ensure flow invariance with increasing Reynolds number. The above critical Reynolds number was originally derived from an isothermal flow across a surface-mounted cube [54]. Although Snyder [54] has warned that "tests to establish Reynolds number independence should be an integral part of any model study," this critical Reynolds number has been incorrectly generalized to other flows (including flows with heat transfer) without questioning its validity. Reduced-scale experiments and full-scale field measurements show that at the same order of Richardson number, the thermal effects are significant only at reduced scale. This means the flow remains a function of Reynolds number, so the Reynolds number independence criterion is invalid. Therefore, in canyon flows with thermal-induced buoyancy, unless the flow is proven independent of both Reynolds number and Grashof number, we should not generalize results from reduced-scale experiments to full-scale street canyons.

Declarations of interest: none

References

[1] J.-F. Sini, S. Anquetin, P.G. Mestayer, Pollutant dispersion and thermal effects in urban street canyons, Atmos. Environ. 30 (1996) 2659–2677.

[2] X. Xie, Z. Huang, J. Wang, Z. Xie, The impact of solar radiation and street layout on pollutant dispersion in street canyon, Build. Environ. 40 (2005) 201–212.

[3] J. Allegrini, V. Dorer, J. Carmeliet, Wind tunnel measurements of buoyant flows in street canyons, Build. Environ. 59 (2013) 315–326.

[4] A. Dallman, S. Magnusson, R. Britter, L. Norford, D. Entekhabi, H.J. Fernando, Conditions for thermal circulation in urban street canyons, Build. Environ. 80 (2014) 184–191.

[5] S. Magnusson, A. Dallman, D. Entekhabi, R. Britter, H.J. Fernando, L. Norford, On thermally forced flows in urban street canyons, Environ. Fluid Mech. 14 (2014) 1427–1441. doi:10.1007/s10652-014-9353-4.

[6] P.-Y. Cui, Z. Li, W.-Q. Tao, Wind-tunnel measurements for thermal effects on the air flow and pollutant dispersion through different scale urban areas, Build. Environ. 97 (2016) 137–151.

[7] Y. Nakamura, T.R. Oke, Wind, temperature and stability conditions in an east-west oriented urban canyon, Atmospheric Environ. 1967. 22 (1988) 2691–2700.

[8] P. Louka, G. Vachon, J.-F. Sini, P. Mestayer, J.-M. Rosant, Thermal effects on the airflow in a street canyon–Nantes' 99 experimental results and model simulations, Water Air Soil Pollut. Focus. 2 (2002) 351–364.

[9] B. Offerle, I. Eliasson, C. Grimmond, B. Holmer, Surface heating in relation to air temperature, wind and turbulence in an urban street canyon, Bound.-Layer Meteorol. 122 (2007) 273–292.

[10] M. Idczak, P. Mestayer, J.-M. Rosant, J.-F. Sini, M. Violleau, Micrometeorological measurements in a street canyon during the joint ATREUS-PICADA experiment, Bound.-Layer Meteorol. 124 (2007) 25–41.

[11] P. Kastner-Klein, E. Fedorovich, M. Rotach, A wind tunnel study of organised and turbulent air motions in urban street canyons, J. Wind Eng. Ind. Aerodyn. 89 (2001) 849–861.

[12] X.-X. Li, D.Y. Leung, C.-H. Liu, K. Lam, Physical modeling of flow field inside urban street canyons, J. Appl. Meteorol. Climatol. 47 (2008) 2058–2067.

[13] L.W. Chew, N. Nazarian, L. Norford, Pedestrian-level urban wind flow enhancement with wind catchers, Atmosphere. 8 (2017) 159.

[14] J.-J. Baik, R.-S. Park, H.-Y. Chun, J.-J. Kim, A laboratory model of urban street-canyon flows, J. Appl. Meteorol. 39 (2000) 1592–1600.

[15] J. Hang, Y. Li, M. Sandberg, R. Buccolieri, S. Di Sabatino, The influence of building height variability on pollutant dispersion and pedestrian ventilation in idealized high-rise urban areas, Build. Environ. 56 (2012) 346–360.

[16] A. Kovar-Panskus, L. Moulinneuf, E. Savory, A. Abdelqari, J.-F. Sini, J.-M. Rosant, A. Robins, N. Toy, A wind tunnel investigation of the influence of solar-induced wall-heating on the flow regime within a simulated urban street canyon, Water Air Soil Pollut. Focus. 2 (2002) 555–571.

[17] N. Nazarian, J. Kleissl, Realistic solar heating in urban areas: air exchange and street-canyon ventilation, Build. Environ. 95 (2016) 75–93.

[18] A.A. Aliabadi, E.S. Krayenhoff, N. Nazarian, L.W. Chew, P.R. Armstrong, A. Afshari, L.K. Norford, Effects of Roof-Edge Roughness on Air Temperature and Pollutant Concentration in Urban Canyons, Bound.-Layer Meteorol. 164 (2017) 1–31.

[19] R.A. Memon, D.Y. Leung, C.-H. Liu, Effects of building aspect ratio and wind speed on air temperatures in urban-like street canyons, Build. Environ. 45 (2010) 176–188.

[20] P.-Y. Cui, Z. Li, W.-Q. Tao, Buoyancy flows and pollutant dispersion through different scale urban areas: CFD simulations and wind-tunnel measurements, Build. Environ. 104 (2016) 76–91.

[21] D. Mu, N. Gao, T. Zhu, CFD investigation on the effects of wind and thermal wall-flow on pollutant transmission in a high-rise building, Build. Environ. 137 (2018) 185–197. doi:10.1016/j.buildenv.2018.03.051.

[22] T. Oke, Boundary layer climates, 2nd edition, Methuen, London and New York, 1987.

[23] J.H. Lienhard V, J.H. Lienhard IV, A heat transfer textbook, Fourth Edition, Dover Publications, Mineola, New York, 2011.

[24] B. Blocken, Y. Tominaga, T. Stathopoulos, CFD simulation of micro-scale pollutant dispersion in the built environment, Build. Environ. 64 (2013) 225–230.

[25] B. Blocken, Computational Fluid Dynamics for urban physics: Importance, scales, possibilities, limitations and ten tips and tricks towards accurate and reliable simulations, Build. Environ. 91 (2015) 219–245.

[26] P.A. Mirzaei, F. Haghighat, Approaches to study urban heat island–abilities and limitations, Build. Environ. 45 (2010) 2192–2201.

[27] S.M. Salim, R. Buccolieri, A. Chan, S. Di Sabatino, Numerical simulation of atmospheric pollutant dispersion in an urban street canyon: comparison between RANS and LES, J. Wind Eng. Ind. Aerodyn. 99 (2011) 103–113.

[28] I. Tolias, N. Koutsourakis, D. Hertwig, G. Efthimiou, A. Venetsanos, J. Bartzis, Large Eddy Simulation study on the structure of turbulent flow in a complex city, J. Wind Eng. Ind. Aerodyn. 177 (2018) 101–116.

[29] Y. Tominaga, T. Stathopoulos, CFD modeling of pollution dispersion in a street canyon: Comparison between LES and RANS, J. Wind Eng. Ind. Aerodyn. 99 (2011) 340–348.

[30] J.-J. Kim, J.-J. Baik, A numerical study of thermal effects on flow and pollutant dispersion in urban street canyons, J. Appl. Meteorol. 38 (1999) 1249–1261.

[31] J. Santiago, A. Dejoan, A. Martilli, F. Martin, A. Pinelli, Comparison between large-eddy simulation and Reynolds-averaged Navier–Stokes computations for the MUST field experiment. Part I: study of the flow for an incident wind directed perpendicularly to the front array of containers, Bound.-Layer Meteorol. 135 (2010) 109–132.

[32] Y. Tominaga, T. Stathopoulos, Numerical simulation of dispersion around an isolated cubic building: model evaluation of RANS and LES, Build. Environ. 45 (2010) 2231–2239.

[33] I. Eliasson, B. Offerle, C. Grimmond, S. Lindqvist, Wind fields and turbulence statistics in an urban street canyon, Atmos. Environ. 40 (2006) 1–16.

[34] G. Vachon, J. Rosant, P. Mestayer, J. Sini, Measurements of dynamic and thermal field in a street canyon, URBCAP Nantes 99, in: Proc. 6th Int Conf Harmon. Atmospheric Dispers. Model. Regul. Purp., 1999: pp. 11–14.

[35] ANSYS Inc, ANSYS FLUENT Theory Guide Release 14.0, (2011).

[36] F. Menter, Best practice: scale-resolving simulations in ANSYS CFD, ANSYS Ger. GmbH. (2012) 1–70.

[37] F. Mathey, D. Cokljat, J.-P. Bertoglio, E. Sergent, Specification of LES inlet boundary condition using vortex method, Prog. Comput. Fluid Dyn. 6 (2006) 58–67.

[38] R. Britter, S. Hanna, Flow and dispersion in urban areas, Annu. Rev. Fluid Mech. 35 (2003) 469–496.

[39] X.-X. Li, C.-H. Liu, D.Y. Leung, Large-eddy simulation of flow and pollutant dispersion in high-aspect-ratio urban street canyons with wall model, Bound.-Layer Meteorol. 129 (2008) 249–268.

[40] S. Hanna, J. Chang, Acceptance criteria for urban dispersion model evaluation, Meteorol. Atmospheric Phys. 116 (2012) 133–146.

[41] ANSYS Inc, ANSYS FLUENT User's Guide Release 14.0, (2011).

[42] H. Werner, H. Wengle, Large-Eddy Simulation of Turbulent Flow Over and Around a Cube in a Plate Channel, in: F. Durst, R. Friedrich, B.E. Launder, F.W. Schmidt, U. Schumann, J.H. Whitelaw (Eds.), Turbul. Shear Flows 8, Springer Berlin Heidelberg, Berlin, Heidelberg, 1993: pp. 155–168.

[43] B. Launder, D. Spalding, The numerical computation of turbulent flows, Comput. Methods Appl. Mech. Eng. 3 (1974) 269–289.

[44] S. Vardoulakis, B.E. Fisher, K. Pericleous, N. Gonzalez-Flesca, Modelling air quality in street canyons: a review, Atmos. Environ. 37 (2003) 155–182.

[45] X. Xiaomin, H. Zhen, W. Jiasong, The impact of urban street layout on local atmospheric environment, Build. Environ. 41 (2006) 1352–1363.

[46] L.W. Chew, A.A. Aliabadi, L.K. Norford, Flows across high aspect ratio street canyons: Reynolds number independence revisited, Environ. Fluid Mech. (2018). doi:10.1007/s10652-018-9601-0.

[47] T. van Hooff, B. Blocken, CFD evaluation of natural ventilation of indoor environments by the concentration decay method: CO2 gas dispersion from a semi-enclosed stadium, Build. Environ. 61 (2013) 1–17.

[48] Y.-K. Ho, C.-H. Liu, M.S. Wong, Preliminary study of the parameterisation of street-level ventilation in idealised two-dimensional simulations, Build. Environ. 89 (2015) 345–355.

[49] Y. Tominaga, T. Stathopoulos, CFD simulations of near-field pollutant dispersion with different plume buoyancies, Build. Environ. 131 (2018) 128-139.

[50] Z. Mo, C.-H. Liu, A wind tunnel study of ventilation mechanism over hypothetical urban roughness: The role of intermittent motion scales, Build. Environ. 135 (2018) 94–103.

[51] X. Xie, C.-H. Liu, D.Y. Leung, M.K. Leung, Characteristics of air exchange in a street canyon with ground heating, Atmos. Environ. 40 (2006) 6396–6409.

[52] N. Ramachandran, B.F. Armaly, T. Chen, Measurements and predictions of laminar mixed convection flow adjacent to a vertical surface, J. Heat Transf. 107 (1985) 636–641.

[53] I. Kovalets, V. Maderich, Numerical simulation of interaction of the heavy gas cloud with the atmospheric surface layer, Environ. Fluid Mech. 6 (2006) 313.

[54] W.H. Snyder, Guideline for fluid modeling of atmospheric diffusion, Environmental Protection Agency, Research Triangle Park, NC (USA), 1981.

[55] F. Bourbia, H. Awbi, Building cluster and shading in urban canyon for hot dry climate: Part 1: Air and surface temperature measurements, Renew. Energy. 29 (2004) 249–262.

[56] M. Santamouris, N. Papanikolaou, I. Koronakis, I. Livada, D. Asimakopoulos, Thermal and air flow characteristics in a deep pedestrian canyon under hot weather conditions, Atmos. Environ. 33 (1999) 4503–4521.